

Indentation Plastometry of Very Hard Metals

Jimmy E Campbell, Marcus Gaiser-Porter, Wenchen Gu, Steve Ooi, Max Burley, James Dean, and Trevor William Clyne*

This investigation concerns the application of profilometry-based indentation plastometry (PIP) to metals with very high hardness, i.e., those with yield stresses of 1.5–3 GPa. The PIP procedure comprises (a) applying a force to an indenter ball, penetrating the sample to a preselected depth, (b) measuring the profile of the indent, and (c) iteratively running a finite element method (FEM) model to obtain the true stress–true strain curve giving optimal agreement between measured and modeled profiles. The procedure is no different when the sample is very hard, although the ball must remain elastic during the process. It is shown that this can be achieved using silicon nitride balls. These can fracture under some conditions, but it is shown that a “proof-testing” operation can be used to ensure that any particular ball will remain elastic under the complete range of service conditions. It is also shown, via systematic comparisons with the outcomes of uniaxial (tensile and compressive) tests, that reliable stress–strain curves can be obtained for very hard metals. Furthermore, PIP testing has advantages over uniaxial testing for obtaining information about their behavior at relatively high strains ($\approx 15\%$), as well as being much easier and simpler to implement.

of PIP to the (instrumented indentation technique) methodology of converting a load–displacement plot to a stress–strain curve via analytic relationships has been clearly demonstrated.^[9] It has already been applied to a thin plasma-sprayed layer^[10] and (anisotropic) additively manufactured material,^[11] both Ni-based superalloys. It has also been confirmed^[12] that residual stresses are unlikely to affect the reliability of extracted stress–strain curves. Important points concerning optimization include the major advantages of a spherical indenter^[5] and the requirement to deform a volume large enough for its mechanical response to be representative of the bulk—usually requiring it to be a “many-grained” assembly. This typically translates into a need for an indenter radius of ≈ 0.5 –1 mm and a load capability in the kilonewton range. This means that “nanoindentation” equipment cannot be used to obtain bulk

properties, and a customized loading frame is required.

An obvious area of interest concerns the testing of very hard metals. Not only do these tend to require high loads, but there is a concern about whether the indenter will remain elastic during the test. Either plastic deformation or cracking would invalidate the test (and any subsequent ones). Indentation of very hard metals inevitably involves the creation of high stresses in the ball. Moreover, these are concentrated in certain regions of the ball and may be regenerated many times. If the ball is taken to be isotropic and homogeneous, and assumed to undergo only conventional plasticity when pushed into a flat sample, then FEM modeling indicates^[13] that such plasticity tends to become significant when the ratio of the yield stress of the ball to that of the sample is no greater than about 2, although there is naturally also a dependence on the load being applied (and hence on the penetration depth). As there is interest in testing metals with yield stresses up to about 3–3.5 GPa, this is potentially an important issue. Moreover, this problem cannot readily be avoided by limiting the applied load (and hence the penetration depth) during the test. To obtain a stress–strain curve that is reliable up to useful levels of plastic strain, the indentation test must involve the generation of strains in an appropriate range, which typically requires the penetration ratio (depth, δ , over indenter radius, R) to be at least around 10%. For a hard sample, this could require loads of at least about 5 kN. There is also the possibility that the microstructure of the ball may not be homogeneous, and that it could undergo other types of deformation or degradation.


1. Introduction

Profilometry-based indentation plastometry (PIP) involves iterative finite element method (FEM) simulation of the indentation of metallic samples, with the plasticity parameters (in a constitutive law) being repeatedly changed until an optimal agreement is reached between experimental and predicted indent profiles. Its emergence is the outcome of an extended period of research and development.^[1–8] The superior reliability

J. E. Campbell, W. Gu, M. Burley, J. Dean, T. W. Clyne
Plastometrex Ltd
204 Science Park, Milton Road, Cambridge CB4 0GZ, UK
E-mail: twc10@cam.ac.uk

M. Gaiser-Porter, T. W. Clyne
Department of Materials Science
University of Cambridge
27 Charles Babbage Road, Cambridge CB3 0FS, UK

S. Ooi
Maxwell Centre
Ovako Group R&D
JJ Thompson Avenue, Cambridge CB3 0HE, UK

 The ORCID identification number(s) for the author(s) of this article can be found under <https://doi.org/10.1002/adem.202101398>.

© 2022 The Authors. Advanced Engineering Materials published by Wiley-VCH GmbH. This is an open access article under the terms of the Creative Commons Attribution License, which permits use, distribution and reproduction in any medium, provided the original work is properly cited.

DOI: 10.1002/adem.202101398

Routine application of PIP requires an integrated system incorporating a loading frame, a profilometer, and a software package that allows automated convergence on the best-fit true stress–strain curve, which can subsequently be used to simulate any loading configuration, including a conventional tensile test. Such an integrated facility is now being produced and sold commercially by Plastometrex Ltd, and this was used in the work described here. Modeling of the indentation must be based on the ball remaining elastic throughout. This article presents an investigation into how this can be ensured when testing very hard metals.

2. Experimental Section

2.1. Materials and Samples

Silicon nitride (Si_3N_4) spheres of 1 mm radius were used, supplied by RPG Balls. Relevant properties quoted by the supplier are presented in **Table 1**. The hardness and compressive strength data, however, need to be treated carefully—not only because their measurement is often problematic but also because their exact meanings, and their relevance to specific loading scenarios, are often unclear.

Five sample materials were used for these tests—all steels with high hardness. Compositions and heat treatments are shown in **Table 2**. Two of them (Maraging 250 and Maraging 350) are well-established maraging steels, supplied by Dynamic Metals. The yield stresses quoted by the supplier are 1.7 and 2.24 GPa, with the higher value for the Maraging 350 being primarily due to the raised Co content. The other three, supplied by Ovako AB, are designated Hybrid 60, 52 100-240, and 52 100-160. These are all designed for bearing applications, usually in the form of relatively large spheres. The 52 100-240 and 52 100-160 are both established high carbon bearing steels with very high hardness—they are certainly among the hardest metals likely to be encountered in engineering usage. The Hybrid 60 steel has been developed more recently, with lower carbon content. Its yield stress is somewhat lower than those of the other two, but it has superior performance in terms of

resistance to corrosion and for usage at elevated temperatures. These benefits are conferred by the presence of relatively high levels of Cr and Al, as well as the lower carbon content. Its hardness is still in a range that makes it suitable for demanding bearing applications.^[14]

2.2. Microstructural Examination

Silicon nitride balls were examined by scanning electron microscope (SEM) (an FEI Nova NanoSEM being operated at 20 kV) after a fracture had occurred during loading. Details of the outcome are given in Section 4.1.

2.3. Tensile Testing of the Steels

Tensile testing of the two maraging steels and the Hybrid-60 was carried out using an Instron 3369, with the machining of the samples done prior to heat treatment. The samples were cylindrical, with a diameter of 5 mm, a reduced section length of 30 mm, and a clip gauge length of 25 mm. The other two steels fail in tension before the ultimate tensile stress is reached. This is consistent with previous work.^[15]

2.4. Compressive Testing of the Steels

Compression tests were carried out on all five steels, again using an Instron 3369 loading frame. Samples were in the form of cylinders (either 3.5 mm diameter and 3.5 mm long or 4 mm by 4 mm). MoS_2 paste was smeared onto both ends, although tests were also carried out with no lubricant. Displacement was measured using a linear variable displacement transducer, attached to the upper platen and actuated against the lower one. Between platens and sample were two alumina plates of thickness 10 mm. The nominal stress–strain curves presented here were corrected for “bedding down” effects by extrapolation of the linear portion back to zero stress, giving the zero strain level. At the end of the test, the “barrelling profile” along the length of the sample was measured with a stylus profilometer.

Table 1. Properties of the silicon nitride balls quoted by the supplier.

Ball spec	Density ρ [Mg m^{-3}]	Young's modulus E [GPa]	Thermal conductivity K [$\text{W m}^{-1} \text{K}^{-1}$]	Thermal expansivity α [K^{-1}]	Vickers hardness H_V [kgf mm^{-2}]	Compressive strength σ_c [GPa]
Si_3N_4 ASTM F2094 Class II	3.26	300	23	3.4×10^{-6}	1400–1600	2.3–4.0

Table 2. Indicative compositions and heat treatments for the five steels.

Designation	Composition										Heat treatment	
	C	Si	Mn	Cr	Ni	Mo	V	Co	Cu	Al	Solution anneal	Temper
Maraging 250	0.03	0.1	0.1	0.5	18.0	5.0	–	8.0	0.05	0.05	–	5 h @ 480 °C
Maraging 350	0.03	0.1	0.1	0.5	18.0	5.0	–	12.0	0.05	0.05	–	5 h @ 480 °C
Hybrid 60	0.28	0.11	0.3	5.32	5.98	0.69	0.49	–	0.16	2.29	45 m @ 1020 °C	4 h @ 545 °C
52 100-240	0.99	0.26	0.28	1.4	0.15	0.04	0.01	–	0.2	0.03	30 m @ 860 °C	2 h @ 240 °C
52 100-160	0.99	0.26	0.28	1.4	0.15	0.04	0.01	–	0.2	0.03	30 m @ 860 °C	1.5 h @ 160 °C

The approach adopted was first to use the PIP procedure to infer the true stress–true strain curve (as a set of parameter values in the Voce constitutive law) —see Section 2.5. These parameter values were then used to simulate both the tensile test and the compression test (with a specified friction coefficient, and incorporating the effect of the presence of the alumina plates). The mesh used for this simulation is shown in **Figure 1a**. This led to nominal stress–nominal strain curves, which could be compared with the corresponding experimental plots. As a further cross-check on the compression data, a comparison was made between measured and modeled barrelling profiles along the length of the sample after the test. This constitutes a sensitive method of estimating the value of the friction coefficient.

2.5. Indentation Plastometry

The PIP setup used in this work is based on the geometry shown schematically in **Figure 1b**. Four steps are involved in obtaining a tensile (or compressive) nominal stress–strain curve from a PIP test. These are as follows: (a) pushing a hard indenter into the sample with a known force, (b) measuring the (radially symmetric) profile of the indent, (c) iterative FEM simulation of the test until the best-fit set of (Voce) plasticity parameter values is obtained, and (d) using the resultant (true) stress–strain relationship in FEM simulation of the tensile or compression test. These steps are described in detail in a recent review paper.^[8]

Samples for indentation were in the form of 8 mm thick plates with lateral dimensions of about 45 by 20 mm. (As the preferred spacing between indents made with a 1 mm radius ball is at least about 4 mm, this allowed up to about 20 indents to be produced on each sample.) It was confirmed that the materials were all isotropic and homogeneous so that single profiles could be taken of each indent (and, in some cases, of the ball). Surfaces for indentation were polished to a 1 μm finish. Applied forces ranged up to 20 kN.

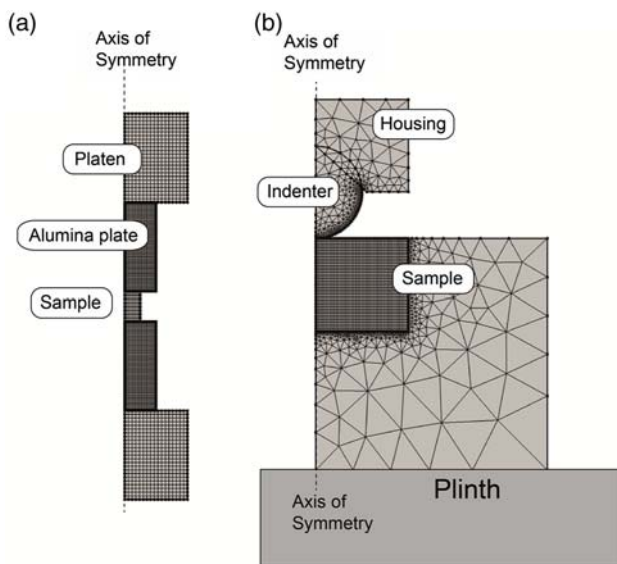


Figure 1. FEM meshes employed for a) compression testing and b) PIP indentation.

3. Uniaxial Testing

3.1. Tensile Curves

Stress–strain curves from the three steels tested in tension are shown in **Figure 2**. The exact shapes of the initial parts of these curves, and the values that might be obtained for yield stress, depend on both the details of exactly how the strain is being measured and the way in which a yield stress value is defined. This applies particularly to the transition regime between elastic and plastic parts, which can be quite sharp, but is sometimes rather gradual. Broadly, however, those for the maraging steels are respectively about 1.8 and 2.3 GPa, which may be compared with figures quoted by the supplier of 1.7 and 2.24 GPa. For the Hybrid 60 steel, the transition to full yielding is more gradual, but most definitions of yield stress would lead to a value around 2.2 GPa. In all three cases, the ultimate tensile stress (UTS) is only slightly above the yield stress, with necking occurring at a strain of just a few percentage.

3.2. Compressive Curves and Barrelling Profiles

Plots of nominal stress against nominal strain, for compression testing of all five steels, are shown in **Figure 3**, with and without lubrication. The lubrication evidently has very little effect, with most of the lubricated plots lying just slightly below the corresponding unlubricated ones. This is not so surprising, as these forces are high and most of the lubrication is probably being squeezed out at an early stage. In fact, this effect tends to create some variability in the elastic part of the plot. Of course, the main outcome of these tests concerns the inferred (true) stress–strain curves for these metals, which requires FEM modeling for accurate assessment (see Section 4.4).

It may also be noted that, with very hard metals of this type, there is a possibility of the sample undergoing some kind of shear band or shear crack formation, invalidating the test.

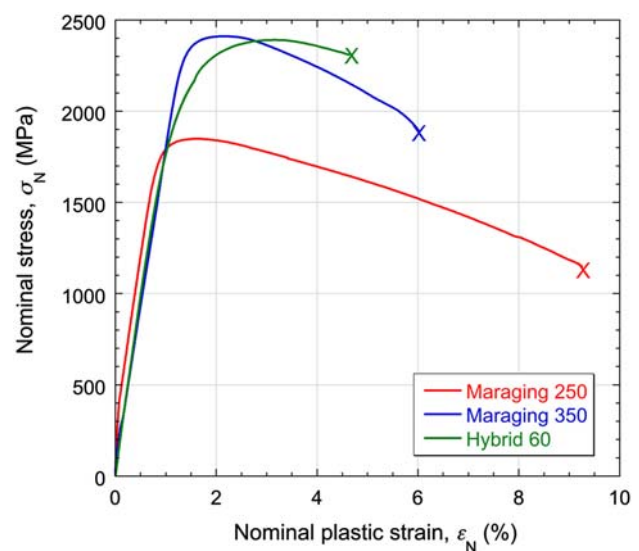


Figure 2. Representative (nominal) stress–strain plots from tensile testing of three steels.

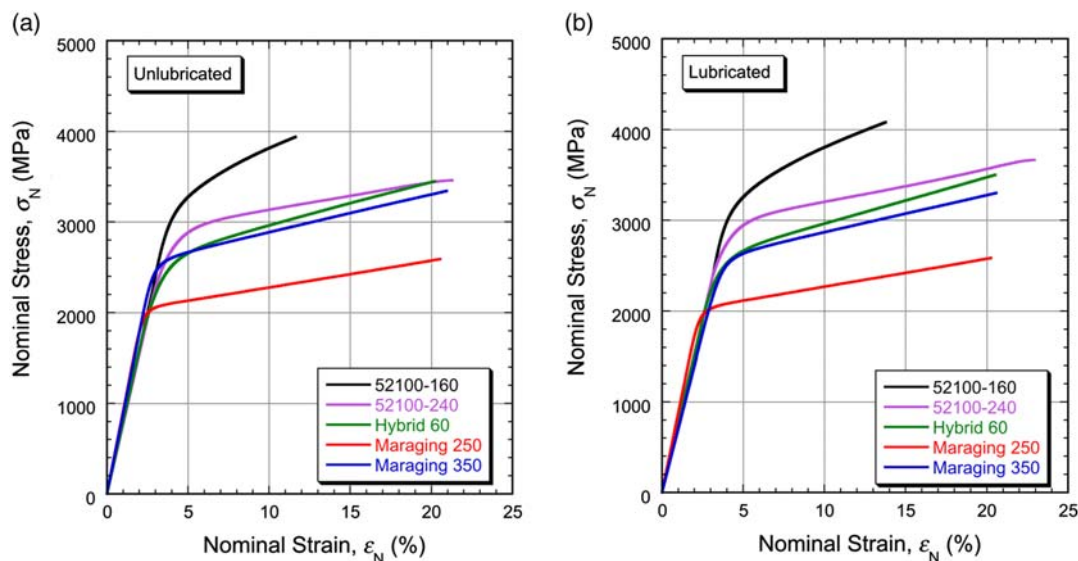


Figure 3. Nominal stress–strain plots from compressive testing of all five steels a) without and b) with lubrication.

There was a tendency for this to happen with the hardest steel, for which tests had to be terminated at relatively low nominal strain levels ($\approx 10\%$ – 15%). It is also important with very hard metals for the samples to be machined to a high level of precision, as any misalignment, or deviation from the loaded surfaces being exactly normal to the loading axis, tends to create significant errors.

While the stress–strain curves show little sensitivity to the lubrication conditions, this is not true for the barrelling profiles, which are shown for two of the steels in **Figure 4**. Evidently, although lubricant gets squeezed out during the test, its presence

does facilitate interfacial sliding, at least during the early stages, and this affects the final barrelling profile. The final lengths of the samples are the same in each case (as the imposed nominal strain was just over 20% in these cases), but more sliding has occurred with the lubricant present, leading to less expansion of the radius as plastic deformation took place. (The final radius at the sample ends was slightly less for the unlubricated samples, as required for the conservation of volume.) This sensitivity means that these measured profiles can be used to estimate the value of the friction coefficient during a particular test (see Section 4.4).

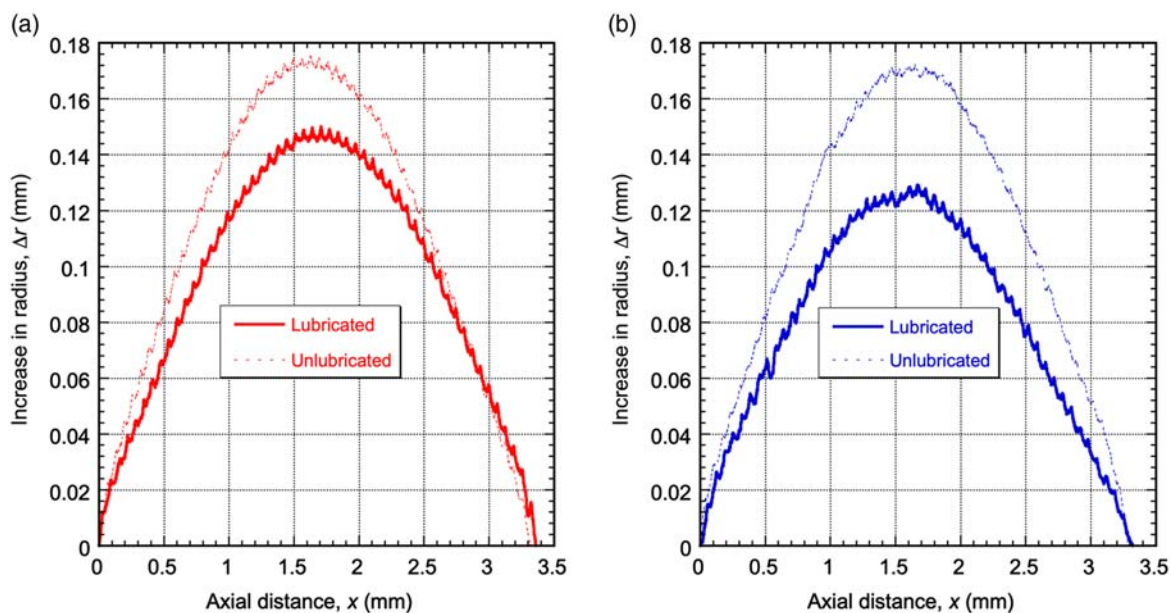


Figure 4. Measured barrelling profiles, with and without lubrication, for a) Maraging 250 and b) Maraging 350 steels. (The undulations are from machining marks on the sample surfaces).

4. Indentation Testing

4.1. Ball Stability

One of the concerns with very hard samples is whether the ball remains elastic during the test. Both plastic deformation and cracking/fracture are unacceptable. For a ceramic, such as silicon nitride, the possibility of plastic deformation can probably be discounted. One way of detecting any such deformation is to monitor the radius of the ball after loading operations (using a profilometer). Such experiments showed that it remained the same (1 mm), to the resolution level of the measurement ($< \approx 1\%$), after all loading operations. The only exception to this was when a catastrophic fracture occurred. Various loading regimes were applied, using Maraging 350 samples. These included the application of progressively increasing loads, up to 20 kN, and up to 20 repeats of a load of 10 kN. Such loading regimes were applied to several different balls. Two of them did fracture. Of course, there must be flaws of some type present in the Si_3N_4 balls and, as their fracture toughness (even their mode II toughness) is unlikely to be very high, unstable failure is possible—depending primarily on the size and location of (small) flaws within the ball. Some ball-to-ball variability is thus expected. However, a “proof-testing” procedure has been developed (involving the application of a higher load than would be used in service, using a very hard sample). This appears to ensure that subsequent failure under service conditions is very unlikely.

It is clearly not a simple matter to predict what is likely to happen to these balls under this kind of loading. A possible approach could be based on their fracture toughness. A review^[16] of such data for Si_3N_4 covers many earlier studies that reported values in the approximate range of 5–9 MPa $\sqrt{\text{m}}$, representing relatively high toughness levels. However, there are at least two problems with these values. The first is that virtually all such measurements were obtained using the Vickers indentation test, which involves measuring the length of cracks running from the corners of the indent. Unfortunately, this method of obtaining a fracture toughness value has been totally discredited.^[17] These

reported values are almost certainly substantial overestimates: as with most ceramics of this type, Si_3N_4 is basically quite brittle.

The second issue, however, is that the loading involved in this application creates little or no mode I driving force for crack propagation, so it is actually a mode II toughness that is required. Such data are in very short supply, but the appropriate value for these materials will certainly be much higher than for mode I. It is therefore difficult to carry out even a semiquantitative analysis of whether the observed behavior is as expected. It should, in any event, be noted that, as mentioned earlier, the key issue here is probably the size of preexisting flaws (and their locations and orientations, relative to the loading axis). Detection and characterization of these prior to service is not really a viable operation, but the proof testing described earlier allows a good level of confidence that they will remain elastic in normal use. The fracture surface of a silicon nitride ball is shown in **Figure 5**, viewed from two angles. While it is often difficult to interpret fracture behavior using stress fields, they can at least be used to explore certain aspects of the behavior and this is done in the following section.

4.2. Stress Fields during Indentation

Some FEM model predictions are shown here, all relating to the application of a load of 10 kN to an Si_3N_4 ball, being pushed into the 52 100-160 steel. **Figure 6** shows the fields of (a) the von Mises stress and (b) twice the peak shear stress, which could be termed the Tresca stress. Both are scalars. Yielding at a particular point would be expected if the value there reached the uniaxial yield stress (according to either the von Mises or the Tresca yielding criterion). This would be relevant for balls made of materials that might be expected to exhibit some plastic deformation (provided an approximate yield stress value is available), but it is not so relevant to the silicon nitride.

However, stress field data can be used as pointers concerning what can in fact happen with the silicon nitride balls. To do this, information is needed about the individual principal stresses. These are shown in **Figure 7**. The first point to note is that there

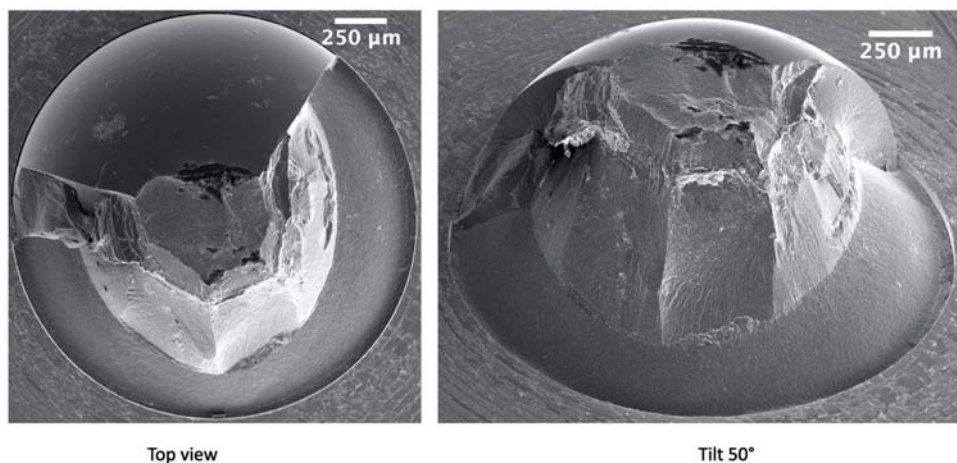


Figure 5. SEM micrographs showing the fracture surface of an Si_3N_4 ball, which had been subjected to a single load of 10 kN, during indenting of the 52 100-160 steel.

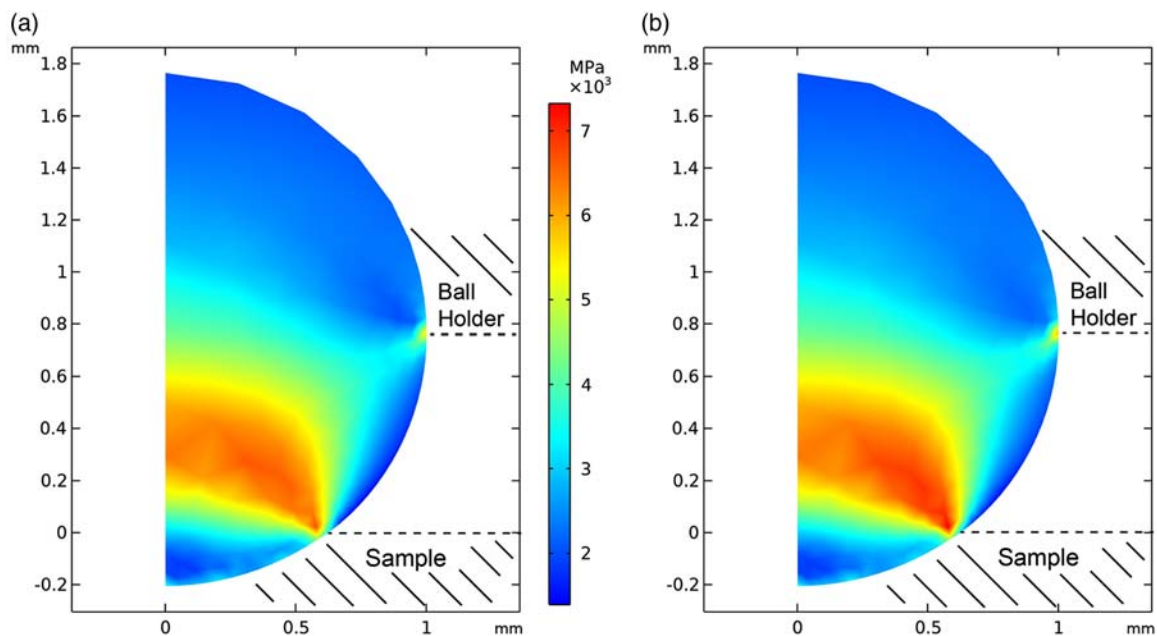


Figure 6. Modeled stress fields within an Si_3N_4 ball, being subjected to a 10 kN load, causing penetration into a 52 100-160 sample. These fields are a) the von Mises stress and b) the Tresca stress (twice the peak shear stress acting at any point).

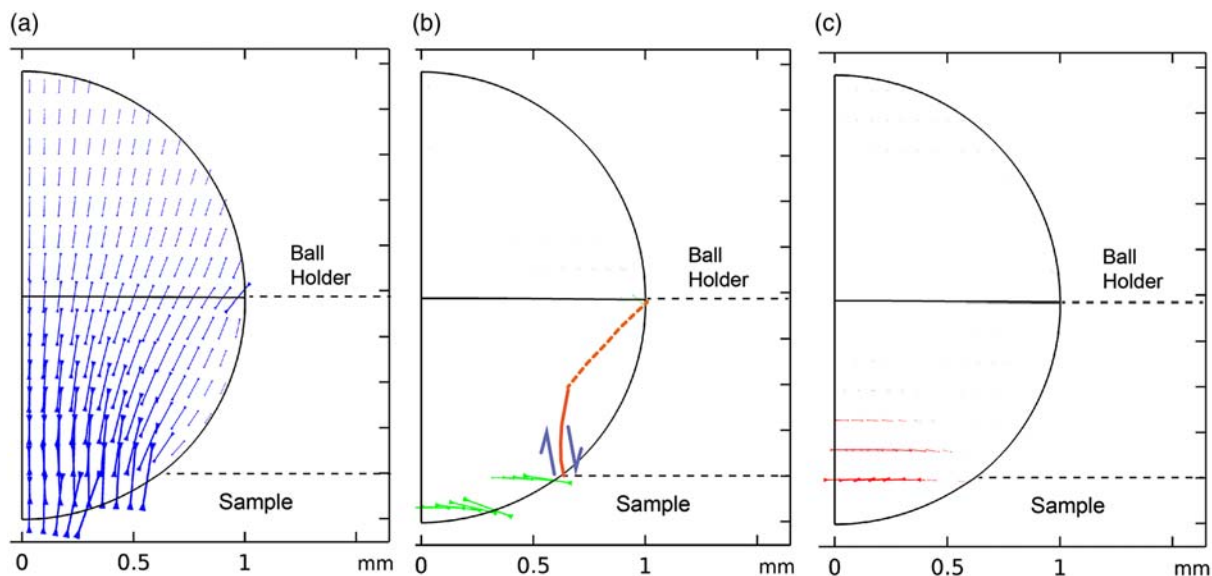


Figure 7. Map of the magnitudes and orientations of the principal stresses within the ball for the simulation of Figure 6, with a,b) being those in the axial-radial plane and c) being those in the hoop direction (normal to the axial-radial plane). Also shown in b) is the approximate path of a mode II (shear) crack propagating from the free surface.

are no significant tensile stresses anywhere. It is therefore clear that no crack propagation can take place under mode I (crack opening mode), at least initially. The focus is therefore on shear stresses that are likely to drive mode II (shear) cracks. The magnitude of these stresses can be seen in Figure 6b and their orientations can be inferred from the principal stress fields shown in Figure 7. As might have been expected, large shear stress acts close to the surface of the ball, at the level of the sample surface. Similar levels extend into the interior of the ball.

The predominant principal stress is compressive, oriented close to the axis of indentation (Figure 7a). The other two are also compressive, but with much smaller magnitudes. Focusing on the shear stresses acting on planes with their normal lying in the axial-radial plane, the approximate path that a mode II crack would be expected to follow is as shown in Figure 7b. The dotted part of this curve shows how the crack path might be expected to deviate as crack advance changes the stress field. As crack growth starts to allow the part of the ball on the “outside” to move

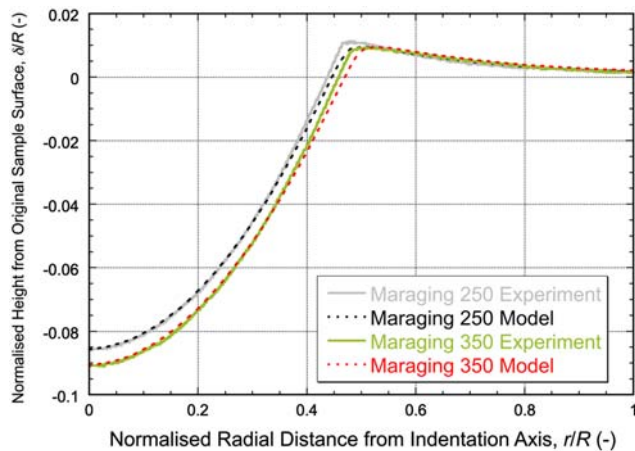


Figure 8. Measured and (best-fit) modeled indent profiles for two of the five steels.

outward, then mode I cracking (or at least crack propagation with an element of mode I driving force) will become possible, allowing the crack to reach the free surface close to the holder. Of course, large parts of the ball will then become detached, leaving a fracture surface of the type shown in Figure 5.

4.3. PIP Testing Outcomes

A comparison is shown in **Figure 8** between measured and modeled indent profiles for two of the steels. The level of agreement was good in all cases. These plots are for single experimental profiles, but the reproducibility was very high, such that repeat runs were virtually identical in all cases. The sets of Voce parameter values corresponding to the best-fit profiles are shown in **Table 3** for all of the steels, while **Figure 9** shows these sets plotted as true stress versus true plastic strain curves, i.e., these are simply plots of the Voce equation.

4.4. Comparisons between PIP and Uniaxial Testing Outcomes

These Voce parameter sets (i.e., a true stress–true plastic strain relationships) can be used (together with the elastic constants) to simulate any loading scenario, including those of uniaxial tensile and compression tests. A comparison between modeled and experimental nominal stress–strain curves is shown in **Figure 10** for the case of tensile testing. This can only be done for three of the five steels, as two of them fracture before

Table 3. Best-Fit Voce plasticity parameter sets for the five steels, obtained from the indent profiles after loading with 1 mm radius silicon nitride balls, creating indents with depths around 100 μm .

Voce parameter	Maraging 250	Maraging 350	Hybrid 60	52 100-240	52 100-160
Yield stress, σ_y [MPa]	1900	2500	2400	2625	2975
Saturation stress, σ_s [MPa]	2200	2800	3400	2825	3575
Characteristic strain, ϵ_0 [%]	20	33	50	50	14

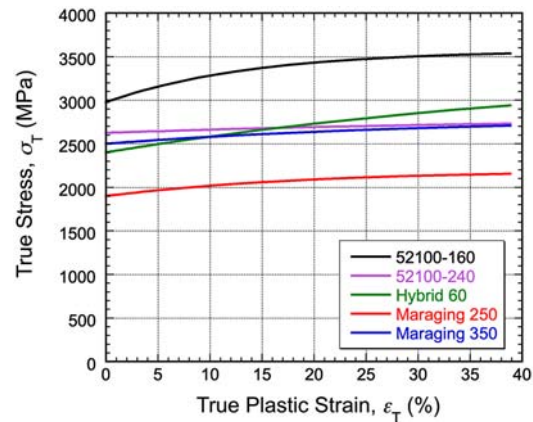


Figure 9. True stress–true strain curves corresponding to the optimized Voce parameter sets in Table 3.

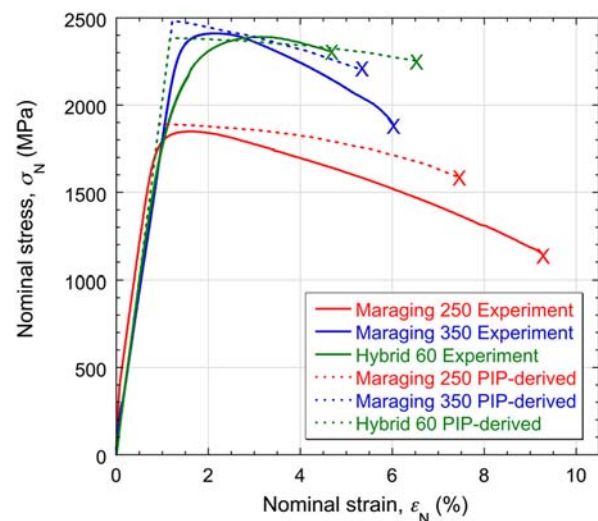


Figure 10. Comparison between tensile nominal stress–nominal strain curves for three steels, as obtained by simulation of the test using PIP-derived true stress–true strain curves and as measured by tensile testing.

yielding—this is always a possibility with very hard materials. The yielding and initial work hardening characteristics have been well captured by the PIP procedure for these three steels. The value obtained experimentally for yield stress will always depend slightly on exactly how it is defined, but, in general, the PIP plots provide accurate representations. There is certainly very little work hardening, so the UTS is close to the yield stress in all cases.

A note should be made regarding the post-necking and final rupture characteristics (“ductility”). Unlike the yielding and UTS (onset of necking), the post-necking response depends on sample dimensions. The true strains in the neck at which rupture was taken to occur are 30% for the two harder steels (Maraging 350 and Hybrid 60) and 50% for the Maraging 250. These values are slightly lower than those typically exhibited by most metals (usually ≈ 50 –100%), but this is broad as expected. In any event,

the general nature of the post-necking behavior of these steels is being captured quite well.

The outcome of the corresponding operation for compression testing is shown in **Figure 11**. The modeling is slightly more complex than for tension, as a value is needed for the friction coefficient. Values have been obtained via the barreling profile comparisons shown in **Figure 12**, leading to the use of 0.15 and 0.2 for lubricated and unlubricated cases, respectively. The sensitivity of stress–strain curves to the value used is low, although

the behavior is significantly different if friction is neglected ($\mu = 0$). The level of agreement is again very good, which provides further confirmation that the PIP-derived true stress–true plastic strain relationships are reliable. There is always some uncertainty associated with the elastic parts of such curves, as the raw data inevitably shows some sort of transition at the beginning—particularly in the presence of lubrication, due to this being progressively squeezed out. For these plots, this was removed by extrapolating the elastic part back to zero stress and taking that

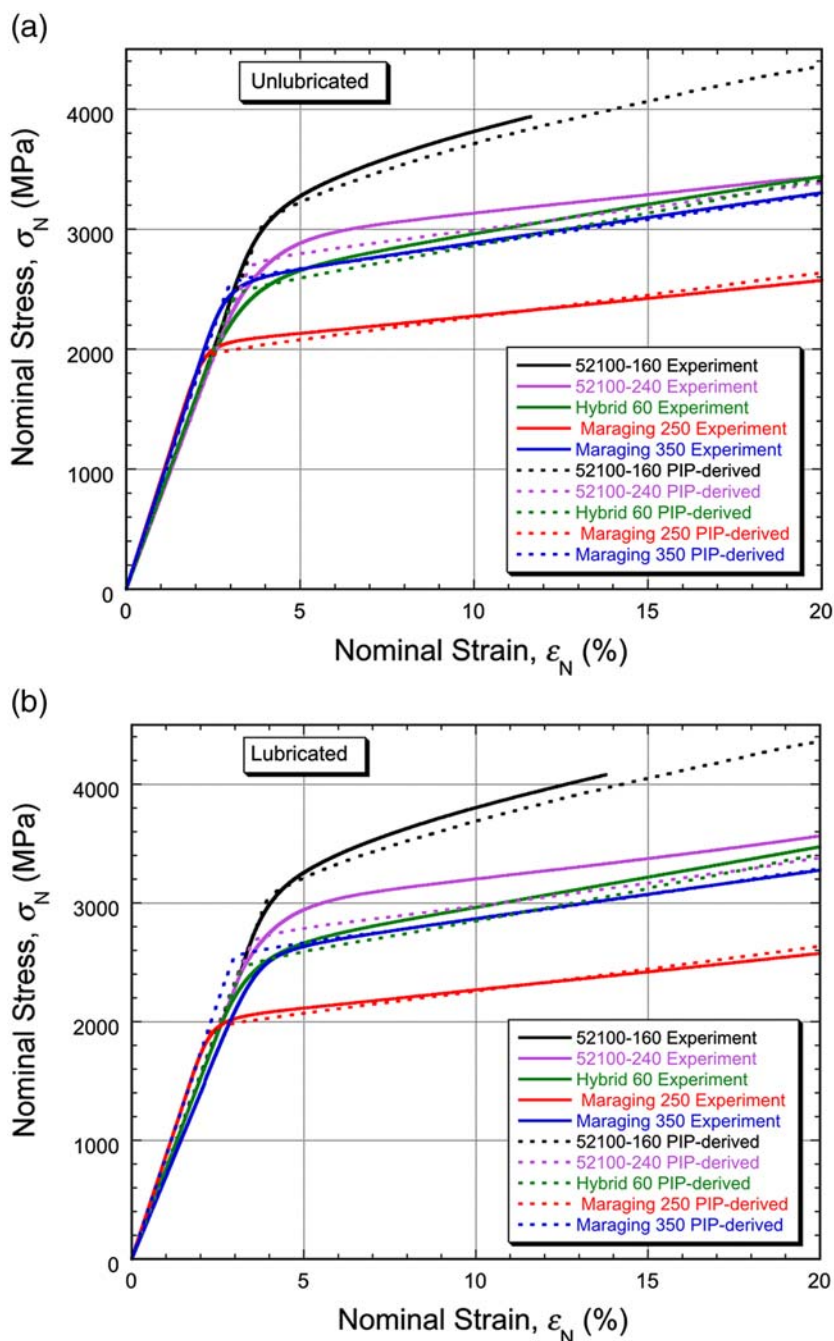


Figure 11. Comparison between compressive nominal stress–nominal strain curves for all five steels, as obtained by simulation of the test using PIP-derived true stress–true strain curves and as measured directly, for a) unlubricated ($\mu = 0.2$) and b) lubricated ($\mu = 0.15$) cases.

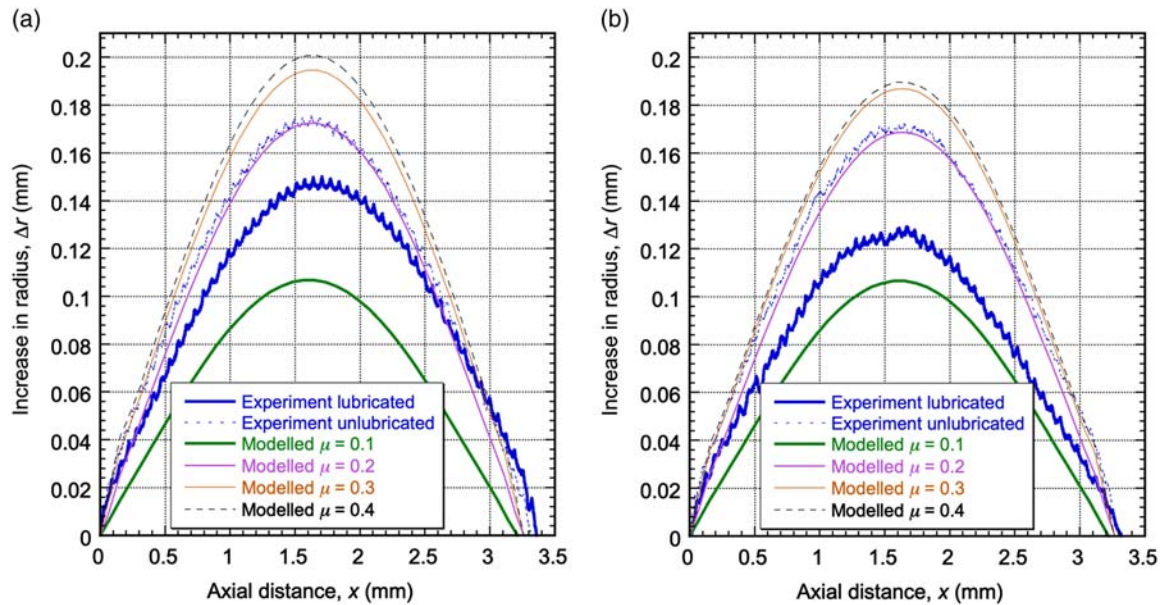


Figure 12. Comparison between measured and modeled barrelling profiles after compressive testing, for a) Maraging 250 and b) Maraging 350.

point as zero strain. This can lead to some variability in this regime. A further point to note is that the observed agreement extends to the two steels that exhibit no tensile ductility. The PIP procedure is thus an excellent way of obtaining the inherent plasticity characteristics of such metals, in a much simpler and easier manner than that of carrying out a compression test and using a bespoke inverse FEM procedure to obtain a true stress–true plastic strain relationship.

4.5. Stress and Strain Fields in the Sample

It is of interest to note the (von Mises) stress and strain fields within a sample during PIP testing. These are shown in

Figure 13 for a sample of 52 100-160, i.e., the hardest steel of those being tested here. This figure confirms that the levels of plastic strain being generated are relatively high (up to about 30%), even for this case, which undergoes more work hardening than the others (see Figure 9), and hence exhibits a tendency for the strain to become more widely dispersed, and for peak strains to be lower. The stress levels are also quite high (up to about 3.5 GPa), as expected from the high load needed to penetrate to the required depth (of about 10% of the ball radius). This capability for interrogating the plasticity characteristics of very hard metals, over a strain range that would be difficult or impossible to cover during uniaxial testing, is potentially an attractive feature of PIP testing.

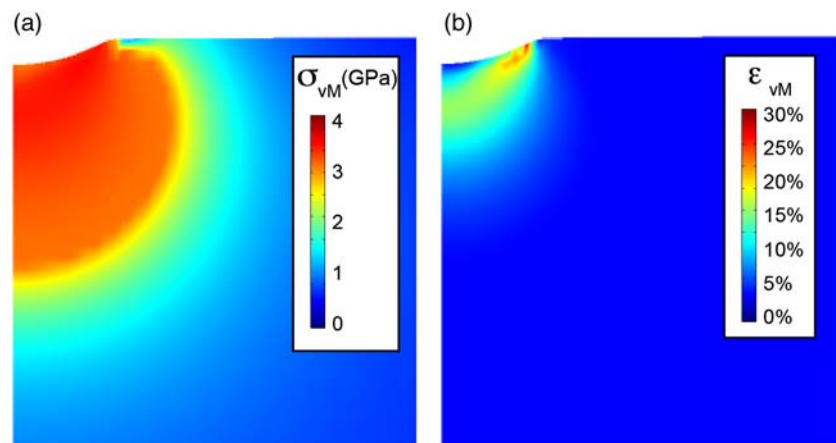


Figure 13. Fields of a) von Mises stress and b) von Mises plastic strain within a 52 100-160 sample being subjected to a load of 7.5 kN via a 1 mm radius silicon nitride ball.

5. Conclusions

Experiments have been carried out on five different types of samples—all steels with yield stresses in the approximate range of 1.8–3.0 GPa. These are among the very hardest metals in common engineering use. They are all isotropic and homogeneous. They have been subjected to uniaxial tensile and compressive testing, as well as PIP testing.

It is shown that there is a high degree of consistency between results obtained from these three types of tests. The fundamental outcome of a PIP test is the relationship between the true von Mises stress and the true plastic von Mises strain. This can be used (via FEM modeling) to predict the outcome of virtually any type of plasticity test, including the nominal stress–nominal strain curves obtained during tensile and compressive testing.

With very hard metals, conventional uniaxial testing presents severe problems. Machining of samples can be difficult, particularly for tensile testing. Also, some such metals can fracture in tension before the yield stress is reached, or shortly thereafter. Furthermore, compressive loading can also present difficulties, with potential for some kind of shear failure at relatively low strains, high sensitivity to any dimensional inaccuracies in the test piece, and a requirement to take careful account of the effect of interfacial friction. In contrast to this, the PIP test allows accurate characterization of the stress–strain relationship, over a relatively large strain range, free of any demanding requirements for sample production or loading alignment.

A key requirement with PIP testing is for the indenter ball to remain elastic throughout. This is potentially an issue when testing very hard metals, particularly as an important aspect of the methodology is that the penetration of the ball into the sample must be a significant fraction ($>\approx 10\%$) of the ball radius, to generate suitable levels of plastic strain. This inevitably leads to high stresses in the ball during the test, although they are predominantly compressive, making fracture less likely. In fact, it is shown that the (silicon nitride) balls being used do not readily undergo either plastic deformation or cracking, even when indenting very hard metals. Fracture is nevertheless possible, occurring mainly under mode II conditions, and this has been investigated. Modeling of the stress fields generated during an indentation test has provided insights into the way that fracture tends to take place. A prior proof-testing procedure is described, which ensures that the ball concerned is very unlikely to fracture under service conditions.

Acknowledgements

Relevant support for TWC has been received from EPSRC (grant EP/1038691/1) and the Leverhulme Trust, in the form of an International Network grant (IN-2016-004) and an Emeritus Fellowship (EM/2019-038/4).

Conflict of Interest

The authors declare no conflict of interest.

Data Availability Statement

The data that support the findings of this study are available from the corresponding author upon reasonable request.

Keywords

finite element method, indentation, plastometry

Received: October 11, 2021

Revised: January 25, 2022

Published online:

-
- [1] C. Heinrich, A. M. Waas, A. S. Wineman, *Int. J. Solids Struct.* **2009**, *46*, 364.
 - [2] J. Dean, J. M. Wheeler, T. W. Clyne, *Acta Mater.* **2010**, *58*, 3613.
 - [3] D. K. Patel, S. R. Kalidindi, *Acta Mater.* **2016**, *112*, 295.
 - [4] J. Dean, T. W. Clyne, *Mech. Mater.* **2017**, *105*, 112.
 - [5] J. E. Campbell, R. P. Thompson, J. Dean, T. W. Clyne, *Mech. Mater.* **2018**, *124*, 118.
 - [6] L. Meng, P. Breitkopf, B. Raghavan, G. Mauvoisin, O. Bartier, X. Herno, *Int. J. Mater. Form.* **2019**, *12*, 587.
 - [7] J. E. Campbell, R. P. Thompson, J. Dean, T. W. Clyne, *Acta Mater.* **2019**, *168*, 87.
 - [8] T. W. Clyne, J. E. Campbell, M. Burley, J. Dean, *Adv. Eng. Mater.* **2021**, *23*, 21004037.
 - [9] J. E. Campbell, H. Zhang, M. Burley, M. Gee, A. T. Fry, J. Dean, T. W. Clyne, *Adv. Eng. Mater.* **2021**, *23*, 2001496.
 - [10] J. E. Campbell, T. Kalfhaus, R. Vassen, R. P. Thompson, J. Dean, T. W. Clyne, *Acta Mater.* **2018**, *154*, 237.
 - [11] Y. T. Tang, J. E. Campbell, M. Burley, J. Dean, R. C. Reed, T. W. Clyne, *Materialia* **2021**, *15*, 101017.
 - [12] M. Burley, J. E. Campbell, R. Reiff-Musgrove, J. Dean, T. W. Clyne, *Adv. Eng. Mater.* **2021**, *23*, 2001478.
 - [13] H. Ghaednia, S. A. Pope, R. L. Jackson, D. B. Marghitu, *Tribol. Int.* **2016**, *93*, 78.
 - [14] J. E. Andersson, F. Lindberg, S. Ooi, in *Bearing Steel Technologies: 12th Volume, Progress in Bearing Steel Metallurgical Testing and Quality Assurance* (Ed: JM Beswick), ASTM, West Conshohocken, PA **2020**, pp. 436–454.
 - [15] R. J. Kar, R. M. Horn, V. F. Zackay, *Metall. Trans.* **1979**, *10A*, 1711.
 - [16] M. H. Bocanegra-Bernal, B. Matovic, *Mater. Sci. Eng. A* **2010**, *527*, 1314.
 - [17] G. D. Quinn, R. C. Bradt, *J. Am. Ceram. Soc.* **2007**, *90*, 673.